FNPF Analysis of Stochastic Experimental Fluid-Structure Interaction Systems

Solomon C. Yim[1]

Huan Lin

Department of Civil Engineering,
Oregon State University,
Corvallis, OR 97331

Katsuji Tanizawa
National Maritime Research Institute,
Tokyo, Japan

A two-dimensional fully nonlinear potential flow model is employed to investigate nonlinear stochastic responses of an experimental fluid-structure interaction system that includes both single-degree-of-freedom surge-only and two-degree-of-freedom surge-heave coupled motions. Sources of nonlinearity include free surface boundary, fluid-structure interaction, and large geometry in the structural restoring force. Random waves performed in the tests include nearly periodic, periodic with band-limited noise, and narrow band. The structural responses observed can be categorized as nearly deterministic (harmonic, sub- and super-harmonic), noisy periodic, and random. Transition phenomena between coexisting response attractors are also identified. An implicit boundary condition upholding the instantaneous equilibrium between the fluid and structure using a mixed Eulerian-Lagrangian method is employed. Numerical model predictions are calibrated and validated via the experimental results under the three types of wave conditions. Extensive simulations are conducted to identify the response characteristics and the effects of random perturbations on nonlinear responses near primary and secondary resonances. [DOI: 10.1115/1.2426990]

Introduction

Much research has been conducted to analytically and experimentally investigate the complex nonlinear responses of compliant ocean structural systems (e.g., [1–5]). For this class of structural systems, they usually possess high degree of nonlinearity in restoring forces and the environmental excitations (e.g., waves, wind, etc.) are random in nature. Because of their large displacements, fluid-structure interaction plays a significant role in both fluid and structural dynamics. In addition, the structural responses are coupled in various degrees-of-freedom.

To keep the analysis manageable, studies often keep only the most dominant motion (e.g., surge), and the wave excitations are assumed deterministic and approximated by simple sinusoidal functions. Even with the simplified models, diverse and complex nonlinear structural responses have been identified to exist (e.g., [6,7]).

Perfect sinusoidal waves are seldom observed in the field and rarely realized in laboratory. A more realistic wave model was introduced by taking into account the presence of random wave components (e.g., [8,9]). Because the presence of randomness in the wave excitation increases the degree of complexity in the analyses, early studies on the nonlinear stochastic responses had been limited to employ semi-empirical, small-body-based, single-degree-of-freedom (SDOF) models (e.g., surge only). Some of the studies modeled random waves by a simple sinusoidal function with additive random components to examine the underlying characteristic responses, and the noise-induced transition and interaction behaviors among those coexisting response attractors (e.g., [8]). Others carried out the studies on the probabilistic properties of nonlinear responses subjected to spectrum-specific random waves (e.g., [9]).

To calibrate these analytical and numerical results, a medium-scale, experimental study of the nonlinear responses of a submerged, moored ocean structure was carried out [10]. In this study, two experimental models, a single-degree-of-freedom (SDOF) in surge only and a two-degree-of-freedom (2DOF) in coupled surge and heave, were employed to examine the response characteristics of each model and their correlations. The tests conducted were intended to be categorized as the deterministic (subjected monochromatic wave excitations) and the stochastic (subjected to random wave excitations). It was, however, noted that the tank noise and other sources of perturbations in waves were present for all tests, and no perfect "deterministic" tests were performed. All the waves generated can then be considered to be stochastic with various degrees of randomness, and experimental responses including both SDOF and 2DOF models exhibited highly nonlinear characteristics.

Based on small body theory, several analytical and numerical models have been developed for experimental response comparisons, both deterministic and stochastic (e.g. [11–13]). Although these predictions show reasonably good agreement, the overly simplified wave conditions and the empirical nature of the formulation governing the fluid-structure interactions were recognized. A more advanced numerical model in better describing both fluid and structural response behaviors and their interactions were strongly recommended.

In this study, we systematically examine and analyze the results of both SDOF and 2DOF experimental, moored, submerged spheres [10]. It is noted that fluid-structure interaction may play a significant role in affecting the response characteristics. Simulations, analyses, and comparisons are carried out from a stochastic perspective, taking into account the random nature of the wave excitations in the experiment reported by Yim et al. [10]. Depending on the source and degree of randomness in the waves, the wave excitations considered in the study are classified as nearly periodic, periodic with random noise, and narrow-band random. A two-dimensional (2-D) fully nonlinear potential flow (FNPF) model is introduced and modified to incorporate the experimental configurations for random wave and structural response simulations. For the FNPF model, the fluid domain is governed by the potential flow theory incorporated with fully nonlinear boundary conditions. A Shinozuka's formulation [14] is employed with the linear wave theory to back-calculate the strokes of a piston-type wavemaker for random wave generation. The waves simulated and compared include nearly periodic, periodic with random per-

[1]Corresponding author.

Contributed by the Ocean Offshore and Arctic Engineering Division of ASME for publication in the JOURNAL OF OFFSHORE MECHANICS AND ARCTIC ENGINEERING. Manuscript received September 29, 2005; final manuscript received September 1, 2006. Assoc. Editor: Rene Huijsmans.

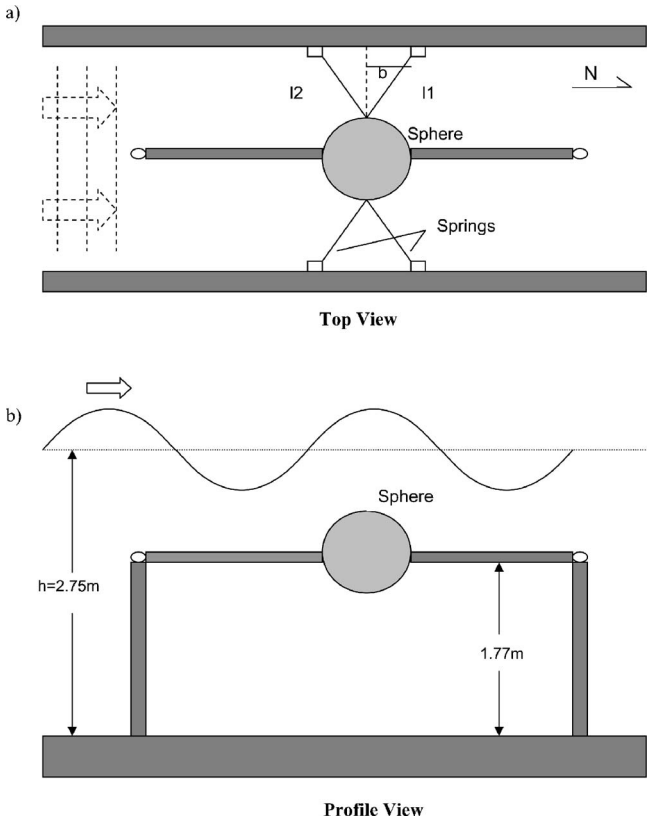

Fig. 1 Experimental SDOF model of a submerged, hydrodynamically damped and excited nonlinear structural system

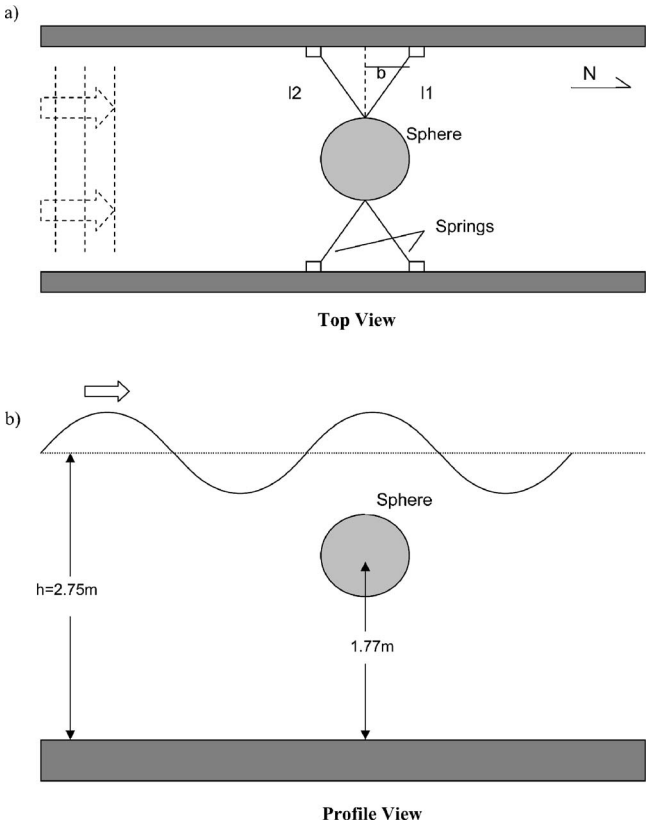

Fig. 2 Experimental 2DOF model of a submerged, hydrodynamically damped and excited nonlinear structural system

turbations, and narrow-band random waves. The sphere is converted to an equivalent cylinder for 2-D computations, and its motions are governed Euler's rigid body motions. Instantaneous equilibrium between fluid and structure is upheld by an implicit boundary condition, and hence fluid-structure interaction is accounted for. Dimensions of the computational fluid domain are constructed for each test based on the wavelength of incident waves. The model simulations are compared with the experimental results in both time and frequency domains. The effects of random perturbations on the response characteristics are further investigated near primary and secondary resonance regions.

Experimental Configurations

The experiment including SDOF and 2DOF configurations was conducted at the O. H. Hinsdale Wave Laboratory at Oregon State University in a wave channel that was 104.3 m long, 3.66 m wide, and 4.57 m deep with a hydraulically driven, hinged flap wave board [10–13]. Data recorded during each test included wave profiles, water particle velocities, sphere displacements, and restoring force on the springs. For reference purpose, a brief description of both SDOF and 2DOF models are presented here. A more detailed description of the model configurations can be found in Yim et al. [10].

SDOF Model Configuration. The SDOF experimental model considered has geometrically nonlinear two-point moored systems with confined motions in the surge (Fig. 1 with $b=0$). The model consists of a neutrally buoyant sphere on a rod supported by guyed masts 2.75 m above the bottom of a closed wave channel. Springs with stiffness of 292 N/m were attached to the sphere at a 90 deg angle to provide a nonlinear restoring force [10]. The damping mechanism includes a linear system (structural) component (associated with the system connections and contact points of instrumentation), a time-dependent Coulomb friction component (due to the setup of restricted surge motion), and hydrodynamic drag. The initial tensions (365 N) in the mooring cables were chosen to ensure nonlinear motion response.

2DOF Model Configuration. The 2DOF experimental model considered in this study has the same configuration as its SDOF counterpart, except that the central rod is removed and the sphere is free to move in all 6 degrees-of-freedom, i.e., surge, heave, pitch, yaw, sway, and roll (Fig. 2). Because of the direction of incident waves and the symmetry of experimental configurations, it was observed that the movement of the sphere was predominantly two dimensional (i.e., surge and heave) with negligible pitch. The energy dissipation mechanism might include structural damping (associated with system connections and contact points of instrumentation) and hydrodynamic drag. The time-dependent Coulomb damping is absent in the 2DOF configuration because of the removal of the rod. The initial tensions in the springs were set to be 111.2 N to ensure nonlinear motion response [10].

FNPF Model of Experimental System

A description of modeling the experimental system employing the fully nonlinear potential flow model is summarized here. The formulation is derived here for the 2DOF experimental configuration, i.e., coupled surge and heave motions for demonstration purpose. The formulation of the SDOF, surge only motions is considered as a limiting case with heave motions equal to zero.

Fluid Domain Formulations. The potential fluid is assumed homogenous, incompressible, inviscid, and its motion irrotational. A representative model of a sample test is shown in Fig. 3. The model has a space fixed $x-z$ axis Cartesian coordinate system with x positive to the right and z negative down and the origin located at the intersection of the at-rest wave-making boundary

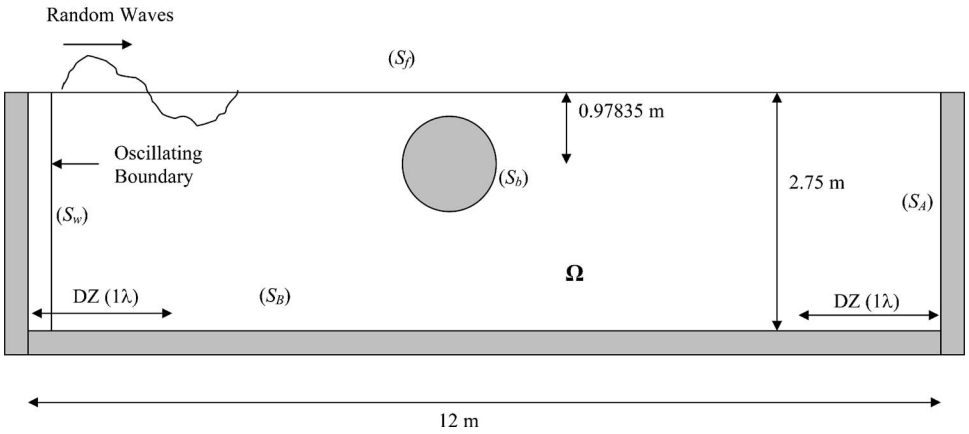

Fig. 3 Two-dimensional numerical wave tank model of a moored, submerged sphere subjected to random waves

and the still water level.

The interior of the tank is the fluid domain (Ω), the fluid boundaries ($\partial\Omega$) are the wavemaker surface (S_w), the absorbing surface (S_A), the free surface (S_f), the bottom boundary (S_B), and the body surface (S_b). The two-dimensional fluid motion $\mathbf{v}(x,z,t)$ can be computed from the positive gradient of the fluid velocity potential, and the pressure $P(x,z,t)$ from the unsteady Bernoulli equation. In the interior of the domain, the velocity potential $\phi(x,z,t)$ and its time derivative $\phi_t(x,z,t)$ satisfy the Laplace's equation.

$$\nabla^2\phi(x,z,t) = 0 \tag{1a}$$

$$\nabla^2\phi_t(x,z,t) = 0 \tag{1b}$$

and the corresponding acceleration potential is given by [15]

$$\Phi = \frac{\partial\phi}{\partial t} + \frac{1}{2}(\nabla\phi)^2 \tag{1c}$$

The acceleration potential is nonlinear in nature and can be directly solved for the pressure exerting on the boundary along the submerged structure. In computations, the velocity potential (Eq. (1*c*)) is formulated and solved for the velocity of fluid particle, which is used to estimate wave profile and compute the boundary condition for the acceleration potential. The acceleration potential is then formulated and solved for the boundary condition and pressure on the surged structure for fluid-structure interaction computations.

Boundary Integral Equations. Boundary integral equations are developed by applying Green's second identity to ϕ and ϕ_t on $S_f \cup S_b$ and are given by

$$c(Q)\begin{Bmatrix}\phi(Q)\\ \phi_t(Q)\end{Bmatrix} = \int_S \begin{Bmatrix}\phi(Q)\\ \phi_t(Q)\end{Bmatrix}\frac{\partial}{\partial n}\ln r(P,Q) - \ln r(P,Q)\begin{Bmatrix}\dfrac{\partial\phi(P)}{\partial n}\\ \dfrac{\partial\phi(P)}{\partial n}\end{Bmatrix} dS \tag{2}$$

where P, Q are points on the boundary, n is the outward normal of the boundary, $r(P,Q)$ is the distance between P and Q, i.e., $\|P-Q\|$ and $c(Q)$ the angle subtended at Q by boundaries.

Boundary Conditions. The fully nonlinear free surface, S_f, boundary condition is given by

$$\frac{D\phi}{Dt} = -\eta + \frac{1}{2}\nabla\phi\bullet\nabla\phi \tag{3a}$$

The bottom boundary is assumed fixed and described as

$$\phi_n = 0 \tag{3b}$$

The body surface (S_b) is assumed to be rigid and impermeable. The body surface boundary condition for the acceleration potential is given by [15]:

$$\frac{\partial\Phi}{\partial\mathbf{n}} = \mathbf{n}\cdot(\dot{\mathbf{V}} + \dot{\omega}\times\mathbf{r}) - k_n(\nabla\phi - \mathbf{V} - \omega\times\mathbf{r})^2 + \mathbf{n}\cdot\omega\times(\omega\times\mathbf{r}) + \mathbf{n}\cdot 2\omega\times(\nabla\phi - \mathbf{V} - \omega\times\mathbf{r}) \tag{3c}$$

where Φ is acceleration potential (Eq. (1*c*)). The first term on the right hand side of the equation is from the body acceleration, the second from the centripetal acceleration of flow on the curved body surface, the third from the centripetal acceleration due to angular velocity of the body, and the last from the Coriolis acceleration. k_n is the normal curvature of the body surface. The free surface is updated by a mixed Eulerian-Lagrangian (MEL) method, which traces the motions of specified fluid particles with velocities computed from the Eulerian formulation ([16]).

Wave Generation. In the FNPF model, waves are generated by an oscillating boundary with specified amplitude and frequency (piston-type of wavemaker). Given designed wave amplitude at specified frequency, the stroke of the oscillating boundary S can be estimated by the linear wave theory. Incorporating with fully nonlinear boundary conditions (Eq. (3)), both linear and nonlinear can be generated. For random wave generation, the wave profile is approximated by applying a Shinozuka's formulation to incorporate all the wave components within the frequency range considered. The resulting stroke of the wavemaker is approximated by a summation of the stroke corresponding to each of the wave components considered.

Stroke of Wavemaker. Shinozuka's formulation is employed to simulate the wave conditions considered in the study, including nearly periodic, periodic with random perturbations, and narrow-band random. The wave profile is then approximated by [14]

$$\eta = \sum_{i=1}^{N}\eta_i = \sum_{i=1}^{N} a_i\cos(\omega_i t + \varphi_i) \tag{4a}$$

where a_i is the wave amplitude at frequency ω_i, and φ_i's are random phases uniformly distributed over $[0\ 2\pi)$. Wave amplitudes a_i's and frequencies ω_i's are determined based on prescribed

wave spectrum. For the amplitude a_i of each wave component, the estimated stroke S_i can be back-calculated by employing linear wave theory [17] and is given by:

$$S_i = \frac{(2\kappa_i h + \sinh 2\kappa_i h)\,\eta_i}{4\sinh^2\kappa_i h \sin(\kappa_i x - \omega_i t)} \tag{4b}$$

where the water depth h, the wave amplitude η, and the wave frequency ω_i are given and the unknown wave number κ_i is determined from the dispersion equation.

The resulting stroke is the summation of the estimated stroke corresponding to each of the harmonic wave components

$$S(t) = \sum_{i=1}^{N} S_i \cos(\omega_i t + \varphi_i) \tag{4c}$$

Note that the wave profile at a given location and the calculations of the phase shifts also account for the difference in the wave traveling speed of each frequency component. In addition, to uphold the accuracy and efficiency of computations, the number of sinusoidal components of the wave maker stroke N is chosen to be 31 for most of the simulations.

Damping Zone. Artificial damping is applied to the ends of the tank to cancel-out reflected waves. Fluxes into the boundary are set equal to zero. In the specified zones, a damping mechanism is applied to the dynamics and kinematics free surface boundary conditions as (e.g., [15])

$$\frac{D\phi}{Dt} = -z + \frac{1}{2}(\nabla\phi)^2 - \nu(x_e)(\phi - \phi_e) \tag{5a}$$

$$\frac{Dx}{Dt} = \nabla\phi - \nu(x_e)(x - x_e) \tag{5b}$$

where $\nu(x_e)$ is the damping coefficient.

Different types of wavemakers used in the experimental system (hinged flap) and in the FNPF numerical model (piston) are noted. In the numerical model, computations and simulations are focused on the domain of interest, typically the middle section of the tank. Only steady-state waves are of interest in the computational domain. Well estimated strokes of the oscillatory boundary would ensure the model simulations are close to the experimental wave profile, and the transient wave formation near the wavemaker, thus the type of wavemaker is relatively insignificant. Numerical results show that the FNPF simulated waves are in very good agreement with the experimental results.

Structure-Equivalent 2-D Cylinder. The sphere is converted to an equivalent cylinder of unit length for 2-D computations. The target radius of the cylinder is formulated by equating the hydrodynamic forces exerting on the sphere and cylinder as given by

$$b = \frac{R}{2}\int_0^{\pi} \cos^2\theta\, d\theta = \frac{\pi}{4}R \tag{6}$$

The weight of the equivalent 2-D cylinder is heavier than the sphere by a factor of $3\pi R/64$. The external forcing excitations, including hydrodynamic, damping, and restoring, are accordingly adjusted to ensure an equivalent dynamic state.

Structural Motions. The motions of the submerged sphere are governed by Euler's equation of a rigid body motion and can be written in vector form as

$$\mathbf{M}\boldsymbol{\alpha} + \beta = \mathbf{F}_f + \mathbf{F}_g \tag{7}$$

$\mathbf{M}$ is the inertia tensor and given by

$$\mathbf{M}\boldsymbol{\alpha} = \begin{bmatrix} m & 0 \\ 0 & m \end{bmatrix} \begin{Bmatrix} \ddot{x}_1 \\ \ddot{x}_2 \end{Bmatrix} \tag{8}$$

where m is the mass of the unit-width cylinder. Surge and heave displacements are represented by x_1 and x_2. β is the gyro moment and a null vector in 2-D computations.

$\mathbf{F}_g$ is the sum of the external forces, consisting of restoring force $\mathbf{R}$ and structural damping force $\mathbf{g}$, and is given by

$$\mathbf{F}_g = \mathbf{R}(\mathbf{x}) + \mathbf{g}(\dot{\mathbf{x}}) = \begin{Bmatrix} R_1(x_1) + g(\dot{x}_1) \\ (x_2) + g(\dot{x}_2) \end{Bmatrix} = \begin{Bmatrix} R_1 + C_1\dot{x}_1 \\ R_2 + C_2\dot{x}_2 \end{Bmatrix} \tag{9a}$$

The restoring forces $\mathbf{R}(\mathbf{x})$ caused by multi-point springs on the submerged circle in surge and heave are respectively given by (e.g., [10])

$$R_1(x_1) = \left[\frac{F_o}{\sqrt{l_0^2 + x_1^2 + x_2^2}} + \left(1 - \frac{l_0}{\sqrt{l_0^2 + x_1^2 + x_2^2}}\right)K\right]x_1$$

$$R_2(x_2) = \left[\frac{F_o}{\sqrt{l_0^2 + x_1^2 + x_2^2}} + \left(1 - \frac{l_0}{\sqrt{l_0^2 + x_1^2 + x_2^2}}\right)K\right]x_2 \tag{9b}$$

where F_o=initial spring tension, ls=initial spring length, $x_{1,2,3}$=cylinder displacement in surge, heave and pitch, respectively, and K=linear spring constant. For the SDOF model, $x_{2,3}=0$.

To better systematically adjust the restoring forces according to the scale factor caused by the 2-D approximation of the sphere (cf. Eq. (6)), a three-term polynomial approximation is introduced:

$$R_1(x_1) \cong k_{11}x_1 + k_{12}x_1^2 + k_{13}x_1^3$$

$$R_2(x_2) \cong k_{21}x_2 + k_{22}x_2^2 + k_{23}x_2^3 \tag{9c}$$

The damping coefficients C_i of the structural damping force $\mathbf{g}$ are given by:

$$C_1 = \xi_1 C_{cr1} = \xi_1(2m\omega_1)$$

$$C_2 = \xi_2 C_{cr2} = \xi_2(2m\omega_2) \tag{9d}$$

where m=mass of the cylinder and $\omega_{1,2}$ and $C_{cr1,2}$=natural frequencies and critical damping coefficients of the system in surge and heave, respectively.

For the SDOF model, the effects caused by the Coulomb friction on the response characteristics may be more significant. When the rod is removed for the 2DOF model, the hydrodynamic drag may play a more prominent role the damping mechanism.

Lastly, $\mathbf{F}_f$ is the generalized hydrodynamic force and can be calculated by

$$\mathbf{F}_f = \int_{S_b} (-\Phi - Z)N\, ds \tag{10}$$

where Φ is the acceleration potential and Z is the distance from the water surface.

Fluid-Structure Interaction. Fluid-structure interaction is governed by an implicit boundary condition upholding the dynamic equilibrium between fluid and body. The implicit boundary condition is given by

$$\phi_{tn} = \mathbf{N}\mathbf{M}^{-1}\left\{\int_{Sb} -\phi_t\mathbf{N}\, ds\right\} + Q \tag{11a}$$

where

$$Q = \mathbf{N}\mathbf{M}^{-1}\left\{\int_{Sb}\left(-z - \frac{1}{2}\nabla\phi\nabla\phi\right)\mathbf{N}\, ds + \mathbf{F}_g - \beta\right\} + q \tag{11b}$$

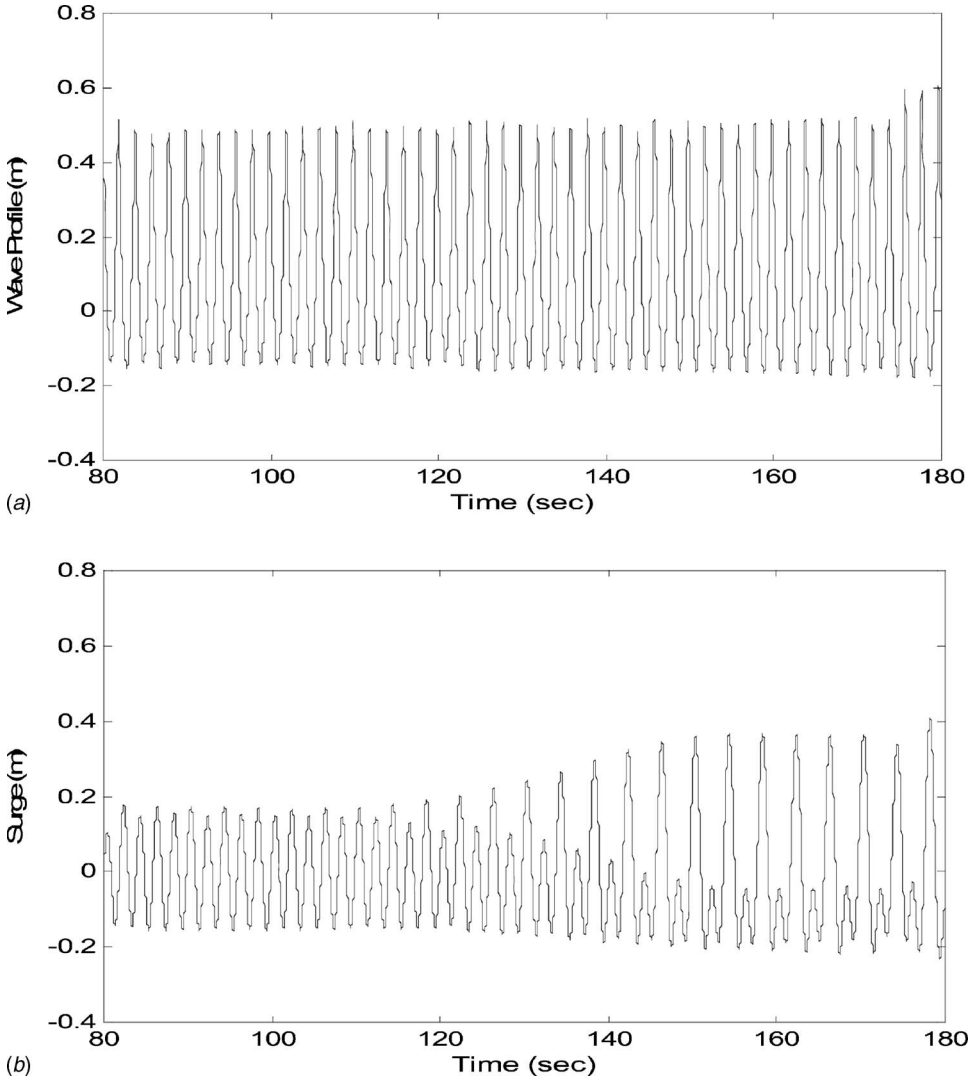

Fig. 4 Transition from SDOF harmonics to subharmonics (test D2): (*a*) wave profile and (*b*) sphere displacement

N is the generalized normal vector of the body surface.

The implicit boundary condition gives the relationship between the acceleration potential and its flux on the body surface. This relation connects kinematic and dynamic conditions and governs the instantaneous equilibrium between the fluid and structure.

Numerical Implementation. A boundary element method (BEM) with collocation point scheme is employed to solve the boundary integral equations (Eq. (2)). The BEM is also directly applied to compute the implicit boundary condition between the fluid and structure (Eq. (11)). A surface fitting technique, e.g., cubic-B spline, is employed for calculations of tangential and normal derivatives. A mesh function is used for arrangement of collocation points for numerical stability. A fourth order Runge-Kutta method time integration is employed. Constant integration time steps are chosen to satisfy the CFL condition [15]; for this specific case, the stability criterion is [18]

$$\Delta t^2 \leq \frac{8\Delta x}{\pi g} \tag{12}$$

The Courant-Friedrichs-Levy (CFL) condition can be explicitly expressed

$$\mu = \frac{\max(\mathbf{v})\Delta t}{\min(\Delta x)} < 1 \tag{13}$$

The depth of the wave tank is kept at 2.75 m for all simulations to maintain experimental wave conditions as well as the dimension of the experiment (Fig. 3). The length of the numerical model is chosen $>4\lambda$ (λ denoting the wavelength of incident waves) to preserve computational accuracy and efficiency. The number of collocation points is 10 on the sides, 40 on the bottom, 120 on the free surface, and 36 on the submerged body. For most cases, the time step is selected as minimum $[T_{wj}/120 T_S/120]$, where T_{wj} is the period of highest-frequency component in the incident wave and T_S is the structural natural period. The cylinder is supported 0.97835 m below the still water level.

For the SDOF model, to ensure the sphere moving in surge-only (therefore SDOF), the hydrodynamic forcing excitation in heave is offset by an artificial, equal force in the opposite direction, which approximates the reacting force caused by the presence of the rod (Fig. 1).

$$F_{g2} = -\sum F_f(x_2) \tag{14}$$

where $F_f(x_2)$ is the resulting exciting forces in the x_2 direction. This restriction is removed for the 2DOF model, and the simulated responses move in surge-heave coupled fashion.

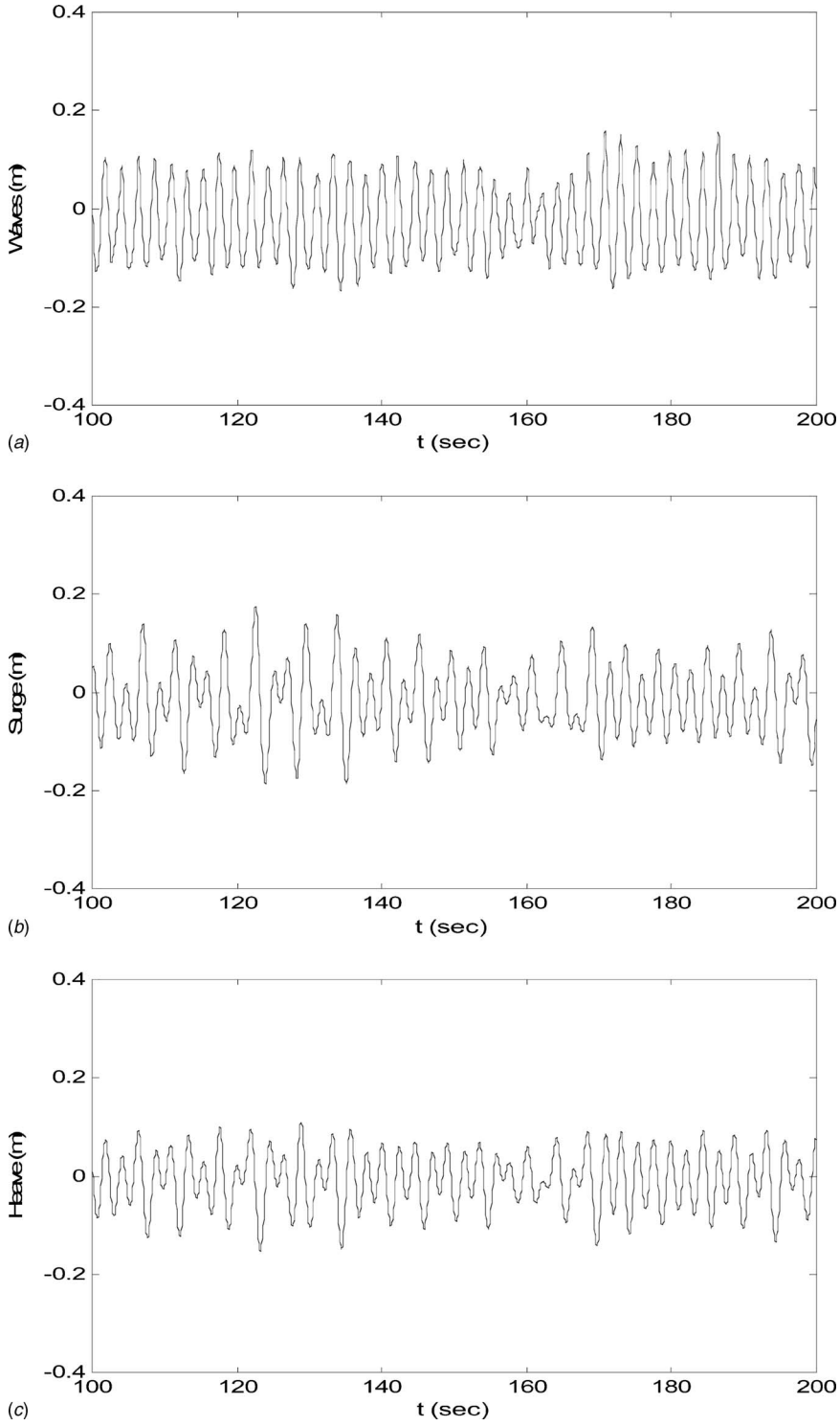

Fig. 5 Sample 2DOF results near subharmonic resonance (test E9): (*a*) periodic waves with additive noise, (*b*) noisy surge, and (*c*) noisy heave

Experimental Results

Random wave excitations to the experimental results can be categorized as nearly periodic, periodic with additive random perturbations, and narrow band. For the tests performed, the dominant wave frequencies were chosen to examine the effects of random wave components on the response characteristics near the identified resonance regions.

Responses Subjected to Nearly Periodic Waves. For the SDOF tests subjected to nearly periodic waves, the period of the dominant wave component ranges among the super-harmonic (test D3), the harmonic (tests D1, D14, and D15), and the sub-harmonic (tests D2 and D9). The 2DOF experimental results also exhibit super-harmonic (tests E4, E5, and E7), harmonic (tests E2, E3, E6, E8, and E13) and sub-harmonic (test E1) responses. Wave conditions in the tests range from shallow water waves near the super-harmonic resonance, linear waves near the harmonic, and nearly nonlinear stokes waves near the sub-harmonic [17].

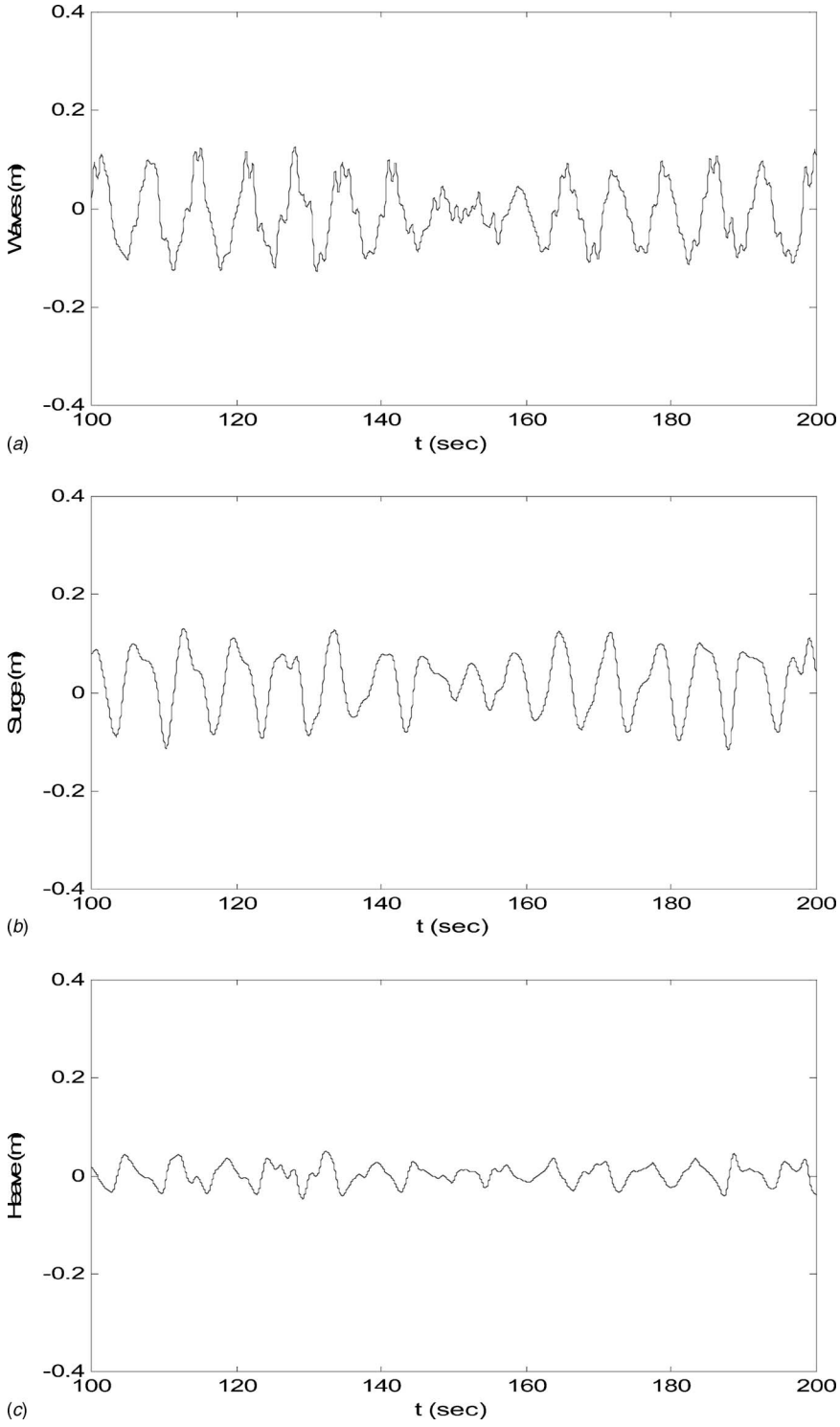

Fig. 6 2DOF experimental results near super-harmonic resonance (test E14): (*a*) periodic waves with additive noise, (*b*) noisy surge, and (*c*) noisy heave response

A SDOF sample of nearly periodic wave profile and its corresponding response time history (test D2) are shown in Figs. 4(*a*) and 4(*b*), respectively. The test was originally designed to be deterministic, however, because of the presence of uncontrollable weak tank noise, variations in wave amplitude are noted (Fig. 4(*a*)). The variations in the wave profile cause a transition between two distinct response modes, from harmonic response to sub-harmonic, observed at around the 120th second in the time history (Fig. 4(*b*)).

Responses Subjected to Periodic Waves With Noise. Designed additive random components were incorporated in the waves to examine the noise effects on the structural response characteristics. For the SDOF tests subjected to periodic waves with random perturbations, the dominant periodic wave components were chosen to be 2 s for all tests (D4–D8 and D11–D13). The intensity of the perturbations is the modulation factor to examine the noise effects on the nonlinear responses. The variance of wave

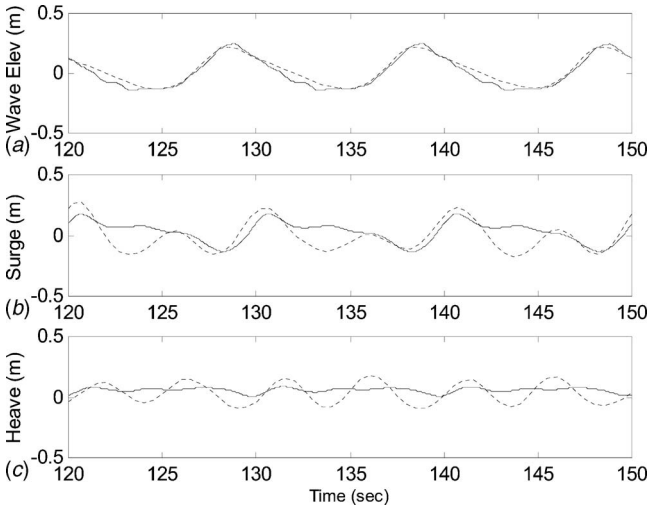

Fig. 7 Comparison of nearly periodic wave profile and super-harmonic responses (test E4): (*a*) wave profile, (*b*) surge, and (*c*) heave displacement; solid line—experimental and dashed line—simulated

perturbations varies between 0.01 and 0.03. The experimental responses all behave in a noisy sub-harmonic fashion. For the 2DOF tests, the period of the dominant wave component is chosen either at 2.22 or 6.67 s to examine the noise effects on the sub-harmonic and super-harmonic responses, respectively. Typical 2DOF sub- and super-harmonic responses subjected to periodic waves with random perturbations are shown in Figs. 5 and 6, respectively.

Responses Subjected to Narrow-Band Random Waves. For the tests subjected to narrow-band random waves, the peak frequencies were chosen to be near the identified nonlinear resonance regions based on deterministic tests. The spectral bandwidth is the modulation factor to further study the response transitional behavior. For SDOF tests (D16–D18), the peak frequency was chosen at 2 s to examine the transitional phenomenon near the sub-harmonic resonance. For the only 2DOF test (E10), the peak frequency was selected at 2.22 s, also near the sub-harmonic domain.

Simulations and Comparisons

The numerical models are calibrated and validated by comparing with the experimental results. Comparisons have conducted for all tests (both SDOF and 2DOF) in either time or frequency domain. Representative tests are selected either from SDOF or

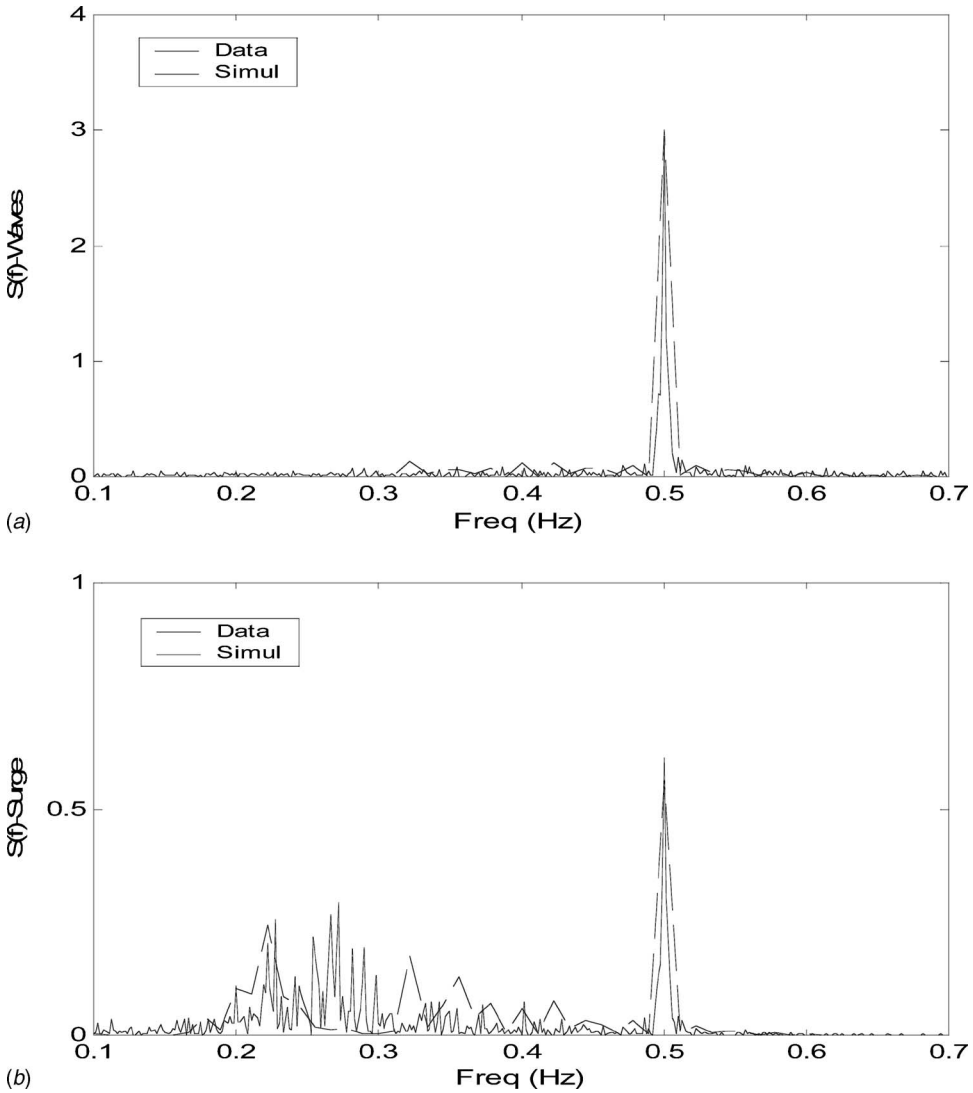

Fig. 8 Comparison of SDOF noisy experimental and simulated results in power spectrum near subharmonic resonance (test D6): (*a*) waves and (*b*) surge response

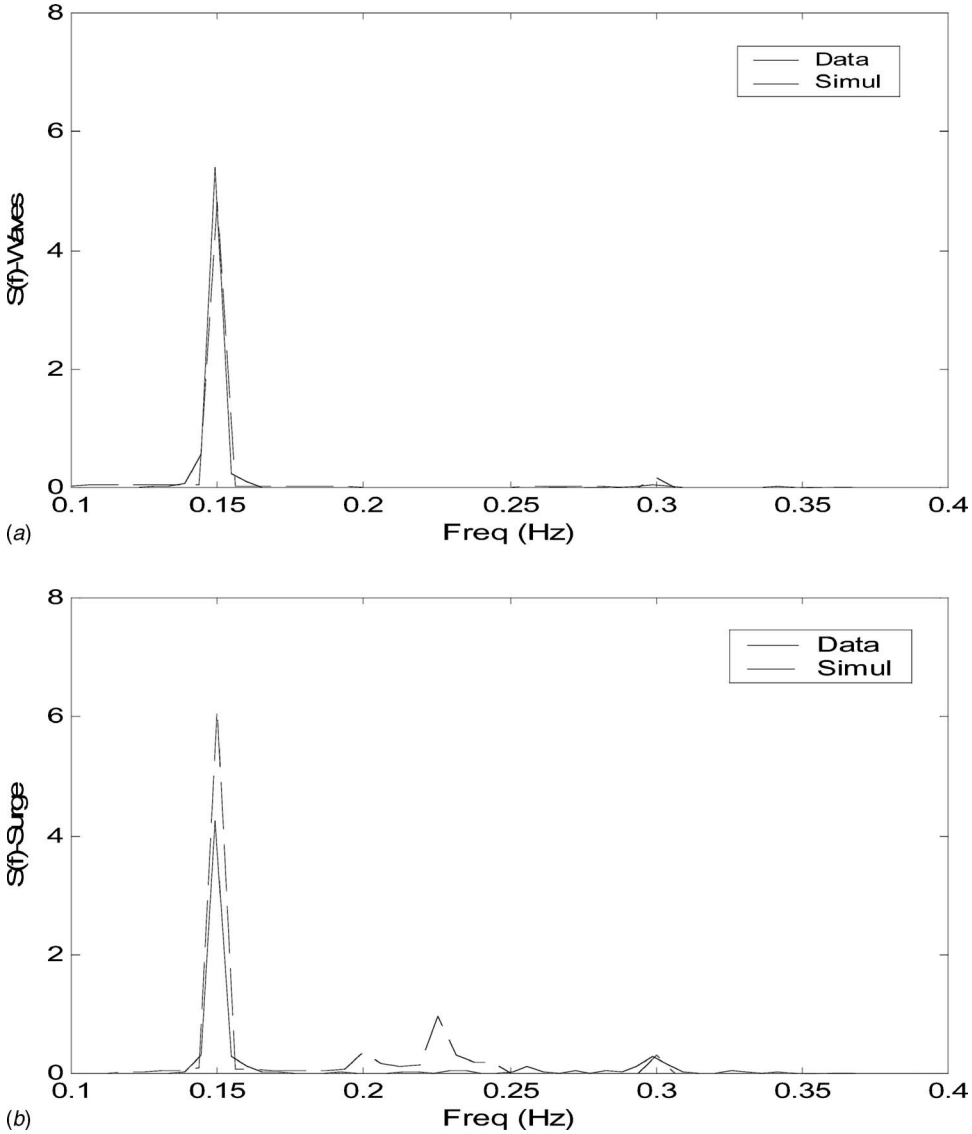

Fig. 9 Comparison of 2DOF noisy experimental and simulated results in power spectrum near super-harmonic resonance (test E14): (*a*) waves and (*b*) surge response

2DOF experimental results for demonstration purpose. Parametric studies with various degrees of randomness in waves also are conducted to examine their effects on nonlinear responses near the primary and second resonances.

Nearly Super-Harmonic Response (2DOF). When the wave excitations are nearly periodic, numerical simulations are in very good agreement with both SDOF and 2DOF experimental results near harmonic and sub-harmonic resonances. The simulated SDOF super-harmonic responses also agree well with the experimental results. However, discrepancies between 2DOF super-harmonic simulations and experimental results are more pronounced.

Comparisons of the 2DOF numerical predictions and experimental results of wave profile, super-harmonic surge, and heave responses (test E4) are shown in Fig. 7. It is observed that the simulations of wave profile, surge, and heave are in agreement with experimental results. The overestimates of predictions in both surge and heave response amplitudes and the differences in characteristic details between the predictions and experimental results are more significant.

These discrepancies may be caused by the approximations of the ideal fluid (inviscid and irrotational) to real fluid, and a 2-D cylinder to a sphere. The 2-D cylinder approximation may be the cause for the difference in response amplitude near the sub-harmonic resonance region. The combined effects of fluid and structure approximations may lead to the less accurate model predictions in the drag-dominant domain [17], near the super-harmonic resonance in this study.

Noisy Sub-Harmonic Response (SDOF). For the SDOF experimental responses, the tests were conducted near the sub-harmonic resonance to examine the effects of noise intensity on the sub-harmonic responses. Sample experimental wave profile and response (test D6) near the sub-harmonic resonance ($\sim$0.5 Hz), and the corresponding FNPF simulations are compared in spectral density shown in Fig. 8. The dominant wave period is around 2 s, and the wave height varies between 0.2 and 0.4 m. Good agreement is shown between the experimental and simulated wave spectral densities (Fig. 8(*a*)). The simulated surge response is also in agreement with the experimental result at the peak frequency in spite of minor discrepancy in energy distributions in the lower (sub-harmonic) frequency range.

Noisy Super-Harmonic Response (2DOF). Noise effects on randomly perturbed super-harmonic experimental responses were

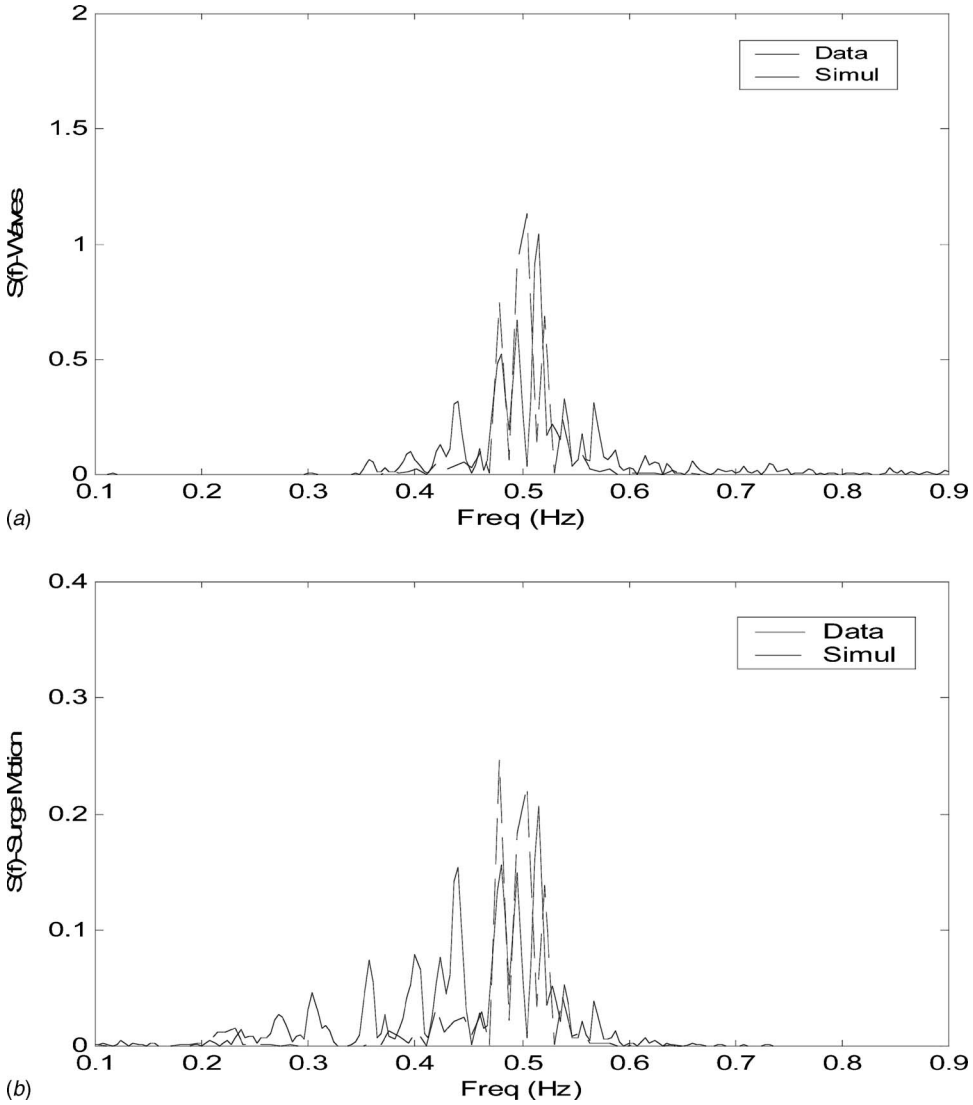

Fig. 10 Comparison of SDOF narrow-band experimental and simulated results in power spectrum (test D16): (*a*) waves and (*b*) surge

conducted in the 2DOF model with wave frequency near a secondary resonance at around 0.125 Hz. Sample experimental wave and super-harmonic surge response, and the corresponding FNPF simulations, are compared and shown in Fig. 9. The numerical results show that the heave motions also closely follow the experimental results, and for the sake of length limit and better demonstration, only surge response is chosen for 2DOF comparisons.

The wave period is around 6.67 s and wave height varies between 0.5 and 0.25 m. The FNPF simulated result is in good agreement with the experimental response in both wave and surge response spectral densities (Figs. 9(*a*) and 9(*b*)). Nonetheless, overestimates of predictions in surge response energy are noted over the frequency range considered (both at the peak and higher frequencies). These results are consistent with the assessment that the 2-D FNPF model with ideal fluid and 2-D structural approximation does not predict the experimental results well near the drag-dominant domain, e.g., near the super-harmonic resonance.

Narrow-Band Random Response (SDOF). All the tests of SDOF and 2DOF models subjected to narrow-band random waves were conducted near their respective sub-harmonic resonances to examine the response characteristics. For better demonstration, sample experimental narrow-band wave profile and response (test D16), and the corresponding FNPF simulations, are compared and shown in Fig. 10. The peak wave frequency is at around 0.5 Hz, and the wave height varies between 0.2 and 0.4 m. Overall agreement is shown between the experimental and simulated responses in both wave and response characteristics.

Parametric Study Near Resonances

Parametric studies are conducted by keeping the total wave energy constant but varying the ratio $\gamma(=a_i/a_p)$ of the amplitude of noise perturbation (a_i's) to the wave amplitude at the peak frequency (a_p). When γ varies from 0 to 1, the characteristic wave excitation varies from periodic to band-limited white noise. The corresponding transitions in response characteristics at the primary and secondary resonances are examined. Large excursions in structural response may exist when the corresponding variance is increased. The results from SDOF and 2DOF models are alternatively selected for most representative demonstrations.

Harmonic Resonance. The primary harmonic resonance locates near 0.25 Hz for SDOF and 0.23 Hz for 2DOF, respectively. The wave excitation of the same total energy with peak frequency near 0.25 Hz transitions from monochromatic to band-limited random wave. Numerical results show both SDOF and 2DOF model response characteristics transitioning in a similar fashion.

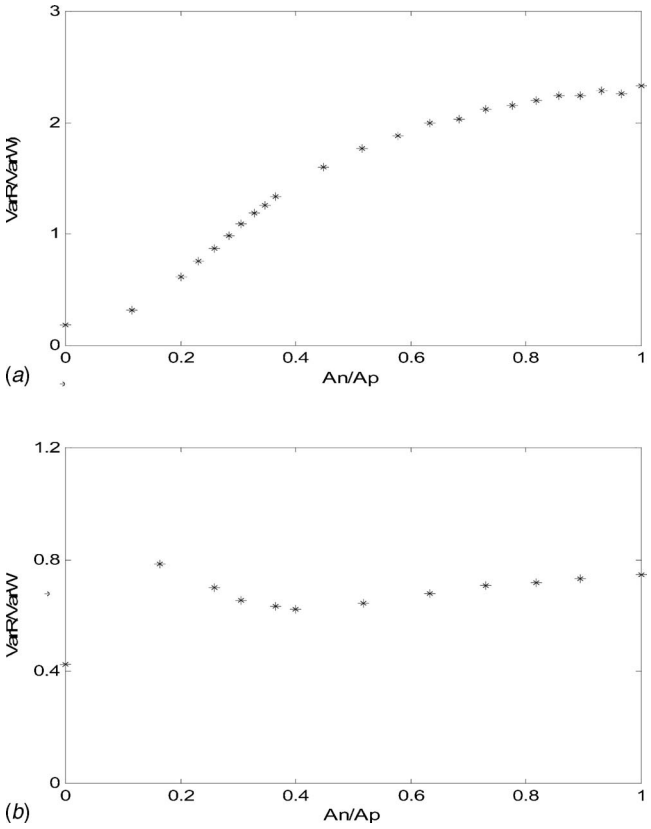

Fig. 11 Response variance versus noise-and-signal ratio near subharmonic resonance: (*a*) SDOF and (*b*) 2DOF

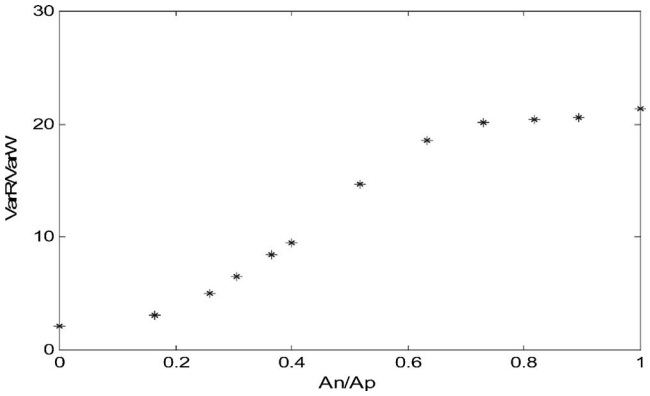

Fig. 12 Response variance versus noise-and-signal ratio near super-harmonic resonance (2DOF)

Sub-Harmonic Resonance. The sub-harmonic resonance locates near 0.5 Hz for SDOF and 0.45 Hz for 2DOF, respectively. The wave excitation of the same total energy with peak frequency near 0.5 Hz varies from periodic to band-limited random wave.

Representative response transitions near the SDOF and 2DOF sub-harmonic resonances are shown in Figs. 11(*a*) and 11(*b*), respectively. For SDOF responses, the response variance increases as the ratio of noise intensity and dominant wave component increases. However, as noted in the 2DOF transition, the response variance jumps when random perturbations are present, decreases when ratio γ reaches 0.4, and then stabilizes. The two distinct trends may reflect the intricate bifurcation pattern near the 2DOF sub-harmonic resonance. Dependency between the variation of response variance and underneath bifurcation pattern is then implied.

Super-Harmonic Resonance. The super-harmonic resonance locates near 0.13 Hz for SDOF and 0.11 Hz for 2DOF, respectively. The wave excitation of the same total energy with peak frequency near 0.12 Hz transitions from monochromatic to band-limited wave. Numerical results show both SDOF and 2DOF model response characteristics transitioning in a similar fashion.

A representative response transition near the SDOF super-harmonic resonance is shown in Fig. 12. The response variance increases when the ratio γ wave component increases. The numerical results indicate that with the same wave excitation energy, a larger excursion can be expected when the random perturbation intensity increases.

Concluding Remarks

A fully nonlinear potential flow (FNPF), 2-D numerical model with random wave generation capability has been formulated to simulate and investigate the results of an experimental fluid-structure interaction system, including both SDOF and 2DOF configurations. The experimental system consisted of a moored, surged sphere subjected to various stochastic wave excitations considered. Major concluding remarks are in the following:

1. Incorporating Shinozuka's formulation, the FNPF model is capable of simulating all random wave conditions considered, including nearly periodic, noisy periodic, and narrow band. The FNPF simulated random wave profiles are in good agreement with experimental results. For the tests subjected to nearly periodic waves, the simulated and experimental waves are compared in the time domain, and for the tests subjected to either periodic with noise or narrow-band random waves, the simulated and experimental results are compared in the frequency domain.
2. For the tests subjected to nearly periodic waves, the FNPF structural response simulations are in good agreement with experimental results in general. Numerical results show that simulations slightly overestimate in amplitude near the secondary resonances, e.g., super- and sub-harmonic. The overestimate is more notable in the lower frequency, super-harmonic regions (drag-dominant).
3. For the tests subjects to periodic waves with noise, good agreement is shown between simulations and experimental results in the frequency domain. The simulations agree with the experimental results at the peak frequencies, and capture the experimental response characteristics at secondary frequency components.
4. For the tests subjected to narrow-band random waves, simulations capture the experimental response characteristics. However, overestimate in amplitude is noted at each frequency component over the frequency range considered.
5. By keeping the wave energy constant and varying the ratio of noise and signal amplitude, transition in response characteristics is examined, and probability of large excursion is inferred. Numerical results show that, in general, probability of large excursion in response increases when the noise and signal amplitude ratio increases. Numerical results also indicate that the increasing trend may depend on the underlying bifurcation pattern near the resonance examined.

The FNPF model adopts the ideal fluid (inviscid and irrotational) model and 2-D cylinder approximation of a 3-D sphere. In the model, the complex energy dissipation mechanism in the experiment system, combined with time-dependent Coulomb friction (SDOF only), structural damping, and drag effect, is approximated by a linear viscous structural damping term. The simplification and approximations may be the causes for the discrepancies between simulations and experimental results, especially notable near the nonlinear resonances (sub- and super-

harmonic). This difference in response amplitude and characteristics is augmented by the more significant drag effects near the super-harmonic domain.

To further improve overall accuracy of model predictions, it is recommended that a 3-D model needs to be developed to better represent the structural (sphere) boundary condition. In the 3-D formulation, a more sophisticated damping model incorporating a time-varying factor should also be considered to closely describe the complex energy dissipation mechanism of the experimental system. Lastly, for more accurate response predictions (especially near the drag-dominant, super-harmonic domain), development of a fluid model incorporating drag effects is also recommended for future research.

Acknowledgment

Financial support from the U.S. Office of Naval Research (Grant Nos. N00014-92-J-1221 and N00014-04-10008) is gratefully acknowledged.

References

[1] Virgin, L. N., and Bishop, S. R., 1988, "Complex Dynamics and Chaotic Responses in the Time Domain Simulations of a Floating Structure," Ocean Eng., **15**, pp. 7–90.
[2] Garza-Rios, L. O., and Bernitsas, M. M., 1995, "Analytical Expressions of the Bifurcation Boundaries for Symmetric Spread Mooring Systems," Appl. Ocean. Res., **17**, pp. 325–341.
[3] Garza-Rios, L. O., and Bernitsas, M. M., 1999, "Slow Motion Dynamics of Turrent Mooring Systems and its Approximation as Single Point Mooring," Appl. Ocean. Res., **21**, pp. 27–39.
[4] Matsuura, J. P. J., Nishimoto, K., Bernitsas, M. M., and Garza-Rios, L. O., 2000, "Comparative Assessment of Hydrodynamics Models in Slow Motion Mooring Dynamics," ASME J. Offshore Mech. Arct. Eng., **122**, pp. 109–117.
[5] Kim, B. K., and Bernitsas, M. M., 2001, "Nonlinear Dynamics and Stability of Spread Mooring With Riser," Appl. Ocean. Res., **23**, pp. 111–123.
[6] Choi, H. S., and Lou, J. Y. K., 1991, "Nonlinear Behavior of an Articulated Loading Platform," Appl. Ocean. Res., **13**, pp. 63–74.
[7] Thompson, J. M. T., 1983, "Complex Dynamics of Compliant Offshore Structures," Proc. R. Soc. London, Ser. A, **387**, pp. 407–427.
[8] Lin, H., and Yim, S. C. S., 1995, "Chaotic Roll Motion and Capsizing of Ships Under Periodic Excitation With Random Noise," Appl. Ocean. Res., **17**, pp. 185–204.
[9] Hsieh, S. R., Troesch, A. W., and Shaw, S. W., 1994, "Nonlinear Probabilistic Method for Predicting Vessel Capsizing in Random Beam Seas," Proc. R. Soc. London, Ser. A, **445**, pp. 195–211.
[10] Yim, S. C. S., Myrum, M. A., Gottlieb, O., Lin, H., and Shih, I.-M., 1993, Summary and Preliminary Analysis of Nonlinear Oscillations in a Submerged Mooring System Experiment, Ocean Engineering Report No. OE-93-03, Oregon State University.
[11] Lin, H., and Yim, S. C. S., 1998, "Experimental Calibration of Bifurcation Superstructure of Nonlinear System," J. Eng. Mech., **124**, pp. 471–475.
[12] Lin, H., and Yim, S. C. S., 1997, "Noisy Nonlinear Motions of a Moored System, Part I: Analysis and Simulations," J. Waterway, Port, Coastal, Ocean Eng., ASCE, **123**, pp. 287–295.
[13] Lin, H., and Yim, S. C. S., 2004, "Stochastic Analysis of a SDOF Nonlinear Moored Experimental System Using an IFF Model," J. Eng. Mech., **130**, pp. 161–169.
[14] Shinozuka, M., 1977, "Simulation of Multivariate and Multidimensional Random Processes," J. Acoust. Soc. Am., **49**, pp. 357–367.
[15] Tanizawa, K., 2000, "The State of the Art on Numerical Wave Tank," *Proc. 4th Osaka Colloquium on Seakeeping Performance of Ships*, Osaka, Japan, October 17–21, pp. 95–114.
[16] Longuet-Higgins, M., and Cokelet, E., 1976, "The Deformation of Steep Surface Waves on Water I. A Numerical Method of Computation," Proc. R. Soc. London, Ser. A, **350**, pp. 1–26.
[17] Dean, R. G., and Dalrymple, R. A., 1984, *Water Mechanics for Engineers and Scientists*, Prentice-Hall, Englewood Cliffs, NJ.
[18] Dommermuth, D., and Yue, D., 1987, "Numerical Simulations of Nonlinear Axisymmetric Flows With a Free Surface," J. Fluid Mech., **178**, pp. 195–219.